Geophysical Journal International

Geophys. J. Int. (2015) **200,** 130–143 doi: 10.1093/gji/ggu377

GJI Geomagnetism, rock magnetism and palaeomagnetism

Thermal magnetic behaviour of Al-substituted haematite mixed with clay minerals and its geological significance

Zhaoxia Jiang,[1] Qingsong Liu,[1] Xiangyu Zhao,[1] Chunsheng Jin,[1] Caicai Liu[2] and Shihu Li[1]

[1]*State Key Laboratory of Lithospheric Evolution, Institute of Geology and Geophysics, Chinese Academy of Sciences, Beijing 100029, China. E-mail: qsliu@mail.iggcas.ac.cn*

[2]*Institute of Geology, China Earthquake Administration, Beijing 100029, China*

Accepted 2014 September 24. Received 2014 September 23; in original form 2014 July 24

SUMMARY

Clay minerals and Al-substituted haematite (Al-hm) usually coexist in soils and sediments. However, effects of clay minerals on Al-hm during thermal magnetic measurements in argon environment have not been well studied. In order to quantify such effects, a series of Al-hm samples were synthesized, and were then mixed with clay minerals (illite, chlorite, kaolinite and Ca-montmorillonite). The temperature dependence of magnetic susceptibility curves in an argon environment showed that Al-substituted magnetite was produced during the thermal treatment via the reduction of Al-hm by the clay mineral, which leads to a significant magnetic enhancement of the thermal products. In addition, the reductive capacity varies among different types of clay minerals, that is, illite > chlorite > kaolinite > Ca-montmorillonite. Furthermore, the iron content in the clay minerals and Al content of Al-hm are two predominant factors controlling the reduced haematite content. The iron is released from the clay minerals and provides the reducing agent, while Al decreases the crystallinity of haematite and thus facilitates the chemical reaction. Therefore, the thermal magnetic measurements can be used to quantify the Al content of Al-hm in natural samples. Our study provides significant information for palaeomagnetism and environmental magnetism studies, such as thermal magnetic analysis and palaeomagnetic intensity reconstruction using ancient pottery and kilns.

Key words: Environmental magnetism; Magnetic mineralogy and petrology; Rock and mineral magnetism.

1 INTRODUCTION

The magnetic properties of minerals are generally temperature dependent, and the Curie and/or Néel temperature (T_c and/or T_N) at which magnetic minerals become paramagnetic is one of the most concerned characteristics since it is effective to identify magnetic minerals (Butler 1992; Dunlop & Özdemir 2001; Liu *et al.* 2012). The curves of saturation magnetization (M_s–T) and temperature-dependence of mass-specific low field magnetic susceptibility (χ–T) are two predominant approaches to obtain T_c (Tauxe 2010; Liu *et al.* 2012). M_s–T curves are generally preferred for determining T_c since M_s is an intrinsic magnetic property independent of grain size and coercivity (Petrovský & Kapička 2006; Tauxe 2010; Fabian *et al.* 2013). In contrast, χ–T curves could provide more detailed insights into environmental information based on the comprehensive investigations and have been widely applied to the studies of Chinese loess-palaeosol sequences (Deng *et al.* 2000; Liu *et al.* 2005), red soil/beds (Liu *et al.* 2010, 2011) and lacustrine or marine sediments (Ortega *et al.* 2006; Bailey *et al.* 2011; Jiang & Liu 2012a; Su *et al.* 2012). However, their interpretation is often complicated by mineral alteration happening during thermal treatments, for example, the dehydration of iron hydroxides (Fe-OOH; Özdemir & Dunlop 1993; Hanesch *et al.* 2006), the transformation of unstable minerals (e.g. maghemite; Roberts 1995; Deng *et al.* 2001) and the reduction or oxidation of some minerals with certain activators (e.g. organics, clay minerals, carbon, etc.; Hanesch *et al.* 2006; Zhang *et al.* 2010, 2012; Minyuk *et al.* 2011), which increase the complexity of the behaviours of the χ–T curves. Therefore, it is essential to investigate the effects of these transformations on behaviours of the χ–T curves.

Clay minerals are particularly abundant in soils (Jackson 1959; Chamley 1989), sedimentary rocks (Zhao & Zhang 1990) and lacustrine/marine sediments (Griffin *et al.* 1968; Thiry 2000). Among these minerals, kaolinite [$Al_2SiO_2O_5(OH)_4$], montmorillonite [$(Ca_{0.33}(Al_{1.67}Mg_{0.33})Si_4O_{10}(OH)_2$, $nH_2O)$], illite [$(K,H_3O)(Al,Mg,Fe)_2(Si,Al)_4O_{10}(OH)_2,(H_2O)$] and chlorite [$(Mg,Fe)_4^{2+}$ $(Fe,Al)_2^{3+}Si_2O_{10}(OH)_8$] are dominant in the Chinese loess/palaeosols, their relative abundance depending on the climate conditions (Thiry 2000). Montmorillonite and kaolinite are more abundant in warm and humid areas, while the other two minerals

Table 1 Summary of properties of the mixed samples.

Sample	Clay mineral added	Clay mineral content (per cent)	H_m mass (g)	χ_0 (m^3 kg^{-1})	χ_{heated} (m^3 kg^{-1})	χ_{heated}/χ_0	Re (per cent)	B_c (mT)	B_{cr} (mT)	M_r (Am^2 kg^{-1})	M_s (Am^2 kg^{-1})
Al0ch0		0	0.2	51.5	6.67	0.13		36.46	116.8	0.16	0.54
Al0ch10	Chlorite	10	0.18	58.68	160.17	2.73	0.22	20.02	68.65	0.21	0.99
Al0ch20	Chlorite	20	0.16	52.86	211.95	4	0.39	20.41	45.16	0.35	1.54
Al0ch30	Chlorite	30	0.14	41.52	179.92	4.33	0.38	19.45	43.26	0.32	1.39
Al0ch40	Chlorite	40	0.12	38	267	7.02	0.74	19.19	36.73	0.5	2.16
Al0ch50	Chlorite	50	0.1	34.37	835.92	24.32	3.12	18.96	33.28	1.77	7.62
Al0ch60	Chlorite	60	0.08	26.38	96.48	3.66	0.34	18.06	47.68	0.13	0.55
Al0ch70	Chlorite	70	0.06	21.29	252.58	11.86	1.5	18.45	32.39	0.51	2.12
Al0ch80	Chlorite	80	0.04	14.92	248	16.62	2.27	18.2	31.47	0.52	2.16
Al0ch90	Chlorite	90	0.02	7.28	241.87	33.22	4.56	17.61	29.93	0.55	2.25
Al0ch98	Chlorite	98	0.004	2.63	196.27	74.63	18.84	15.25	27.5	0.3	1.42
Al4ch0		0	0.2	70.79	69.65	0.98		86.3	120.3	0.24	0.39
Al4ch10	Chlorite	10	0.18	42.48	50.87	1.2	0.01	59.23	111	0.22	0.49
Al4ch30	Chlorite	30	0.14	24.67	308.19	12.49	0.57	33.22	54.94	0.95	2.8
Al4ch50	Chlorite	50	0.1	23.84	70.94	2.98	0.13	39.99	73.54	0.23	0.62
Al4ch60	Chlorite	60	0.08	14.24	196.6	13.81	0.64	30.11	52.35	0.54	1.71
Al4ch80	Chlorite	80	0.04	11.6	327.3	28.22	2.23	15.21	31.17	0.49	0.03
Al4ch85	Chlorite	85	0.03	5.375	336.98	62.69	3.12	29	48.23	1.18	3.84
Al4ch90	Chlorite	90	0.02	8.72	228.53	26.21	3.1	27.71	46.85	0.63	2.1
Al4ch92	Chlorite	92	0.016	3.73	231.17	61.98	4.02	29.26	48.82	0.79	2.53
Al4ch94	Chlorite	94	0.012	2.54	187.47	73.81	4.35	29.16	48.61	0.61	1.97
Al4ch96	Chlorite	96	0.008	2.89	178.35	61.71	6.2	27.25	46.77	0.64	2.19
Al4ch98	Chlorite	98	0.004	4.99	191.74	38.42	13.19	26.57	46.62	0.45	1.63
Al4mon10	Ca-montmorillonite	10	0.18	27.32	29.82	1.09	0.004				
Al4mon30	Ca-montmorillonite	30	0.14	22.56	19.76	0.88	0.005				
Al4mon50	Ca-montmorillonite	50	0.1	16.18	14.28	0.88	0.005				
Al4mon70	Ca-montmorillonite	70	0.06	14.72	16.287	1.11	0.007	71.5	110.5	0.07	0.14
Al4mon80	Ca-montmorillonite	80	0.04	12.24	18.03	1.47	0.04	52.44	90.84	0.07	0.15
Al4mon90	Ca-montmorillonite	90	0.02	7.662	23.74	3.1	0.23	36.76	65.16	0.09	0.26
Al4mon98	Ca-montmorillonite	98	0.004	5.34	20.67	3.87	1.08	26.78	47.33	0.06	0.19
Al4kao10	Kaolinite	10	0.18	25.88	29.65	1.15	0.006				
Al4kao30	Kaolinite	30	0.14	18.64	22.69	1.22	0.008				
Al4kao50	Kaolinite	50	0.1	16.27	15.8	0.97	0.001				
Al4kao70	Kaolinite	70	0.06	9.12	134	14.69	0.59				
Al4kao80	Kaolinite	80	0.04	14.22	92.169	6.48	0.55	32.54	54.99	0.35	1.04
Al4kao90	Kaolinite	90	0.02	10.66	53.53	5.02	0.61	33.38	56.04	0.19	0.57
Al4kao98	Kaolinite	98	0.004	4.35	14.39	3.31	0.71	33.47	56.71	0.04	0.12
Al4il10	Illite	10	0.18	31.47	182.86	5.81	0.24	35.94	64.24	0.52	1.56
Al4il20	Illite	20	0.16	33.92	482.48	14.22	0.79	32.62	53.39	1.42	4.25
Al4il30	Illite	30	0.14	21.92	437.97	19.98	0.84	31.95	52.17	1.32	3.97
Al4il50	Illite	50	0.1	20.93	679.17	32.45	1.86	29.24	46.3	2.08	6.28
Al4il60	Illite	60	0.08	12.18	531.32	43.62	1.83	30.62	49.89	1.4	4.3
Al4il80	Illite	80	0.04	14.4	706	49.03	4.88	30.55	49.53	2.3	7.49
Al4il90	Illite	90	0.02	14.13	708.33	50.13	9.81	31.8	51.68	1.94	6.2
Al4il98	Illite	98	0.004	7.75	177.4	22.89	11.98	26.82	45.91	0.46	1.73
Al8ch0		0	0.2	35.05	33.61	0.96		94.3	148	0.26	0.28
Al8ch10	Chlorite	10	0.18	18.98	26.13	1.38	0.02	71.89	135.9	0.13	0.28
Al8ch30	Chlorite	30	0.14	14.71	818.62	55.65	3.28	24.19	43.41	1.37	5.37
Al8ch50	Chlorite	50	0.1	10.11	514.7	50.91	2.88	21.08	38.95	0.86	3.65
Al8ch60	Chlorite	60	0.08	8.361	600.83	71.86	4.23	23.55	41.52	1.1	4.33
Al8ch80	Chlorite	80	0.04	6.8	359.88	52.92	5.04	19.69	38.12	0.63	3.02
Al8ch85	Chlorite	85	0.03	4.88	296.86	60.83	5.56	20.37	39.43	0.59	2.76
Al8ch90	Chlorite	90	0.02	4.8	369.3	76.94	10.41	20.42	37.38	0.73	3.19
Al8ch92	Chlorite	92	0.016	1.88	258.18	137.33	9.15	20.2	37.55	0.53	2.33
Al8ch94	Chlorite	94	0.012	1.05	366.2	348.76	17.38	19.71	36.59	0.76	3.24
Al8ch96	Chlorite	96	0.008	2.57	267.94	104.26	18.96	19.38	35.99	0.58	2.44
Al8ch98	Chlorite	98	0.004	6.957	230.9	33.19	31.99	19.76	35.58	0.45	1.99
Al12ch0		0	0.138	7.6	7.3	0.96		142.2	233.7	0.21	0.38
Al12ch10	Chlorite	10	0.18	13.8	12.7	0.92	0.01	189.5	269	0.18	0.31

Table 1 (*Continued*).

Sample	Clay mineral added	Clay mineral content (per cent)	H_m mass (g)	χ_0 ($m^3\ kg^{-1}$)	χ_{heated} ($m^3\ kg^{-1}$)	χ_{heated}/χ_0	Re (per cent)	B_c (mT)	B_{cr} (mT)	M_r ($Am^2\ kg^{-1}$)	M_s ($Am^2\ kg^{-1}$)
Al12ch20	Chlorite	20	0.16	13.95	447.27	32.06	4.92	40.77	56.94	2.27	5.15
Al12ch30	Chlorite	30	0.14	12.84	122.04	9.5	1.42	36.37	50.1	0.6	1.33
Al12ch40	Chlorite	40	0.12	10.83	232.19	21.44	3.35	33.68	45.52	1.02	2.31
Al12ch50	Chlorite	50	0.1	7.53	92.9	12.34	1.55	32.86	46.35	0.45	1.02
Al12ch60	Chlorite	60	0.08	8.16	415.07	50.87	9.25	31.68	43.54	1.67	3.87
Al12ch70	Chlorite	70	0.06	7.44	278.08	37.38	8.2	32.06	44.09	1.29	2.98
Al12ch80	Chlorite	80	0.04	4.96	179.89	36.27	7.95	30.84	41.61	0.76	1.75
Al12ch85	Chlorite	85	0.03	3.97	247.85	62.43	14.78	31.4	45	0.4	2.52
Al12ch90	Chlorite	90	0.02	1.967	194.07	98.66	17.46	29.43	40.18	0.75	1.76
Al12ch92	Chlorite	92	0.016	2.1	196.14	93.4	22.05	30.43	43.85	0.83	2.01
Al12ch94	Chlorite	94	0.012	1.72	184.87	107.48	27.75	29.78	42.98	0.81	1.98
Al12ch96	Chlorite	96	0.008	1.24	172.87	139.41	39.01	28.5	41.18	0.7	1.73
Al12ch98	Chlorite	98	0.004	2.03	158.1	77.88	70.94	25.44	36.32	0.59	1.52

Notes: Sample name, for example, Al0ch0, where Al is aluminium, the number following Al is Al substitution of haematite in mol%, 'ch' is the abbreviate of chlorite, and the number after 'ch' is the mass percentage of chlorite in the mixed samples. In addition, 'mon', 'kao' and 'il' are the abbreviates of Ca-montmorillonite, kaolinite and illite.

χ_0 and χ_{heated} are magnetic susceptibility before and after heating, while χ_{heated}/χ_0 is the susceptibility enhancement after heating.

Re is proposed to indicate the reduced percentage of haematite, which is illustrated as $Re = (X_{heated} - X_0)/X_{Hm}/[X_{mt}/X_{Hm} - 1] \times 100\%$, was proposed, where X_{Mt} and X_{Hm} are the magnetic susceptibilities of magnetite and haematite.

Table 2. The chemical analysis of the original clay minerals used in this study.

Clay mineral	Content (per cent)										
	SiO_2	Al_2O_3	TiO_2	Fe_2O_3	FeO	MnO	MgO	CaO	Na_2O	K_2O	P_2O_5
Kaolinite	44.2	39.7	1.39	0.98	0.15	0.002	0.03	0	0.013	0.05	0.034
Ca-montmorillonite	52.8	15.7	0.181	1.06	0.05	0.03	7.98	0.95	0.92	0.03	0.02
Chlorite	49.8	6.63	0.45	2.59	1.25	0.01	29.88	0.59	0.16	0.03	0.05
Illite	49.3	24.25	0.55	7.32	0.55	0.03	2.56	0.43	0	0.03	0.03

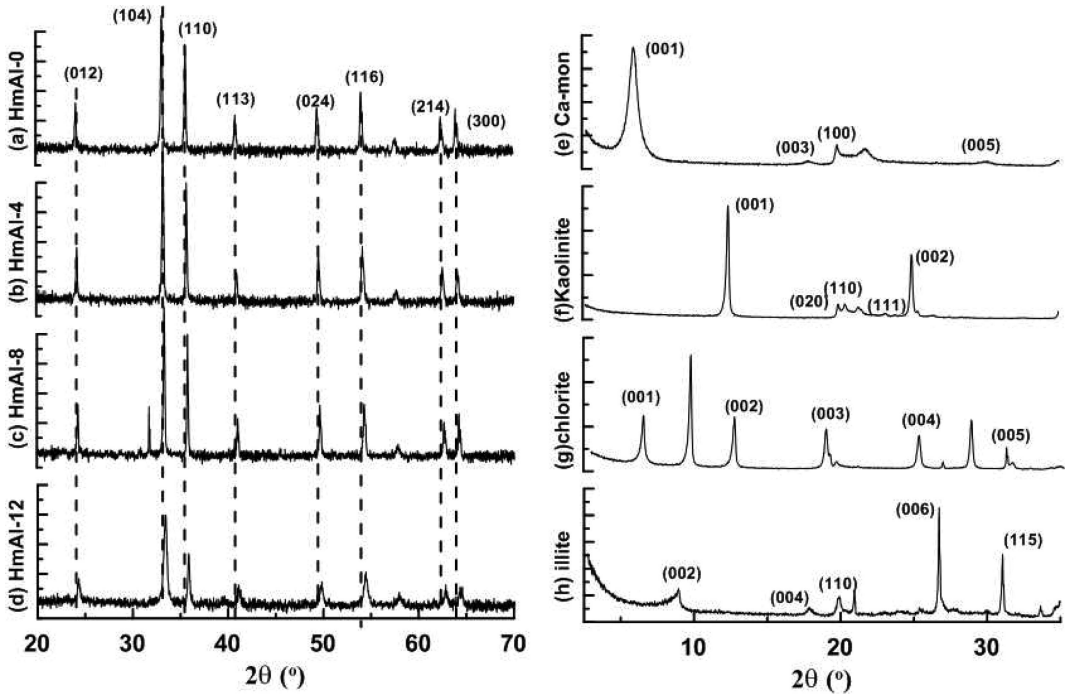

Figure 1. X-ray diffraction (XRD) data for the original clay minerals and Al substituted haematite (Al-hm). (a)–(d) The XRD data for Al-hm samples, where the number following Al represents the Al content in mol% (Al/(Al+Fe)×100 per cent) added into the initial prepared solutions; (e)–(h) the XRD data for clay minerals.

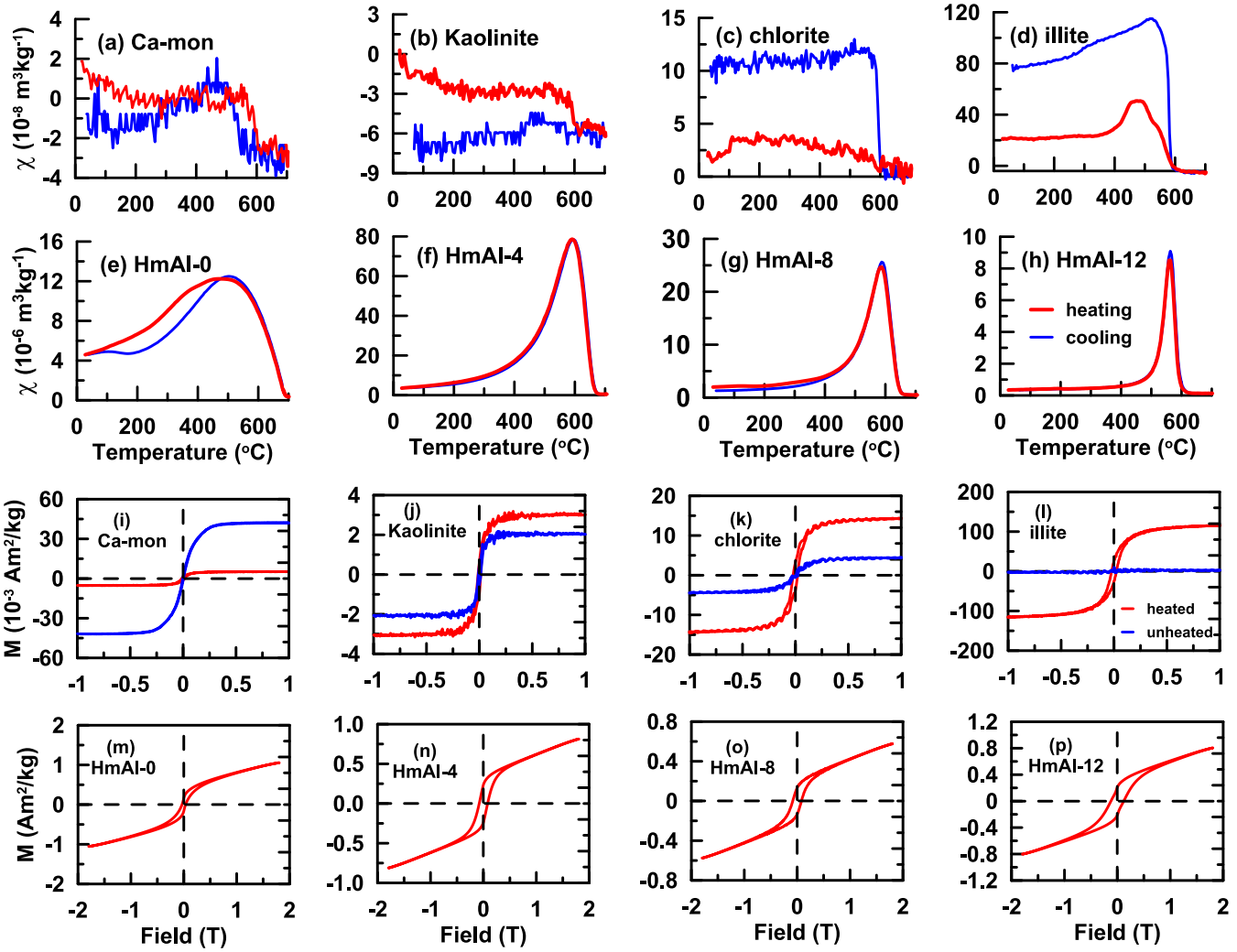

Figure 2. The magnetic properties of the raw clay minerals and Al-hm samples. (a)–(d) The temperature dependence of magnetic susceptibility curves (χ–T) for clay minerals; (e)–(h) χ–T curves for Al-hm samples, where the red and blue lines represent the heating and cooling curves, respectively; (i)–(l) the magnetic hysteresis loops for original clay minerals, where the blue and red lines stand for the loops measured before and after heating, respectively; (m)–(p) the magnetic hysteresis loops for Al-hm samples.

are prone to be well preserved in hot-dry or cold regions. This is a consequence of strong hydrolysis in wet areas that leads to the weathering of illite/chlorite but the neoformation of kaolinite/smectite (Chamley 1989; Zhao & Zhang 1990; Peng & Guo 2007). Therefore, it is suggested that the illite crystallinity is a good palaeoclimatic proxy for the summer monsoon evolution (Bronger & Heinkele 1990; Ji *et al.* 1999; Zhao *et al.* 2005) and that the chlorite content is a preferred indicator for the chemical weathering intensity of soils (Ji *et al.* 1999; Zhao *et al.* 2005).

It is well known that many magnetic minerals (e.g. haematite, goethite and maghemite) are associated with clay minerals in sediments and soils (Cornell & Schwertmann 2003). For example, haematite, as the predominant pigment, has been detected in red soils/beds by magnetic and spectroscopic methods (Walker 1967; Collinson 1974; Kiipli *et al.* 2000). The direct observation of transmission electronic microscopy (TEM) reveals that haematite is usually surrounded by clay minerals in Chinese loess/palaeosols (Chen *et al.* 2010). Given to the reducibility of clay minerals (Zhang *et al.* 2012), the reaction between haematite and clay minerals is considered responsible for the magnetic enhancement of samples (Liu *et al.* 2005). In a control study, Zhang *et al.* (2012) reported the similar magnetic enhancement after heating of mixtures of pure haematite and chlorite in argon that demonstrates the reduction of haematite to magnetite by chlorite is a likely mechanism. In natural samples, however, haematite is usually substituted by aluminium (Al), which has remarkably different properties from pure haematite (Schwertmann *et al.* 1977; Murad & Schwertmann 1986; Jiang *et al.* 2012). Therefore, we synthesized a series of Al-substituted haematite (Al-hm) samples with varying Al content to investigate the thermal magnetic behaviours of the mixtures of Al-hm and clay minerals. In addition, thermal magnetic measurements of natural red soil/beds samples were also performed to compare with that of the synthetic samples.

2 EXPERIMENTS

In this study, we used four types of commercial clay minerals, that is kaolinite, Ca-montmorillonite, illite and chlorite, and synthetic Al-hm. Al-hm samples were synthesized by the transformation of akaganéite (β-FeOOH) at 95 °C. Akaganéite suspensions were prepared by mixing 250 ml of 0.4 M (Fe, Al) $(NO_3)_3$ with 1 M sodium hydroxide (NaOH) to a final pH of 7 (Sugimoto & Sakata 1992). The initial Al content added to the solution was 0, 4, 8 and 12

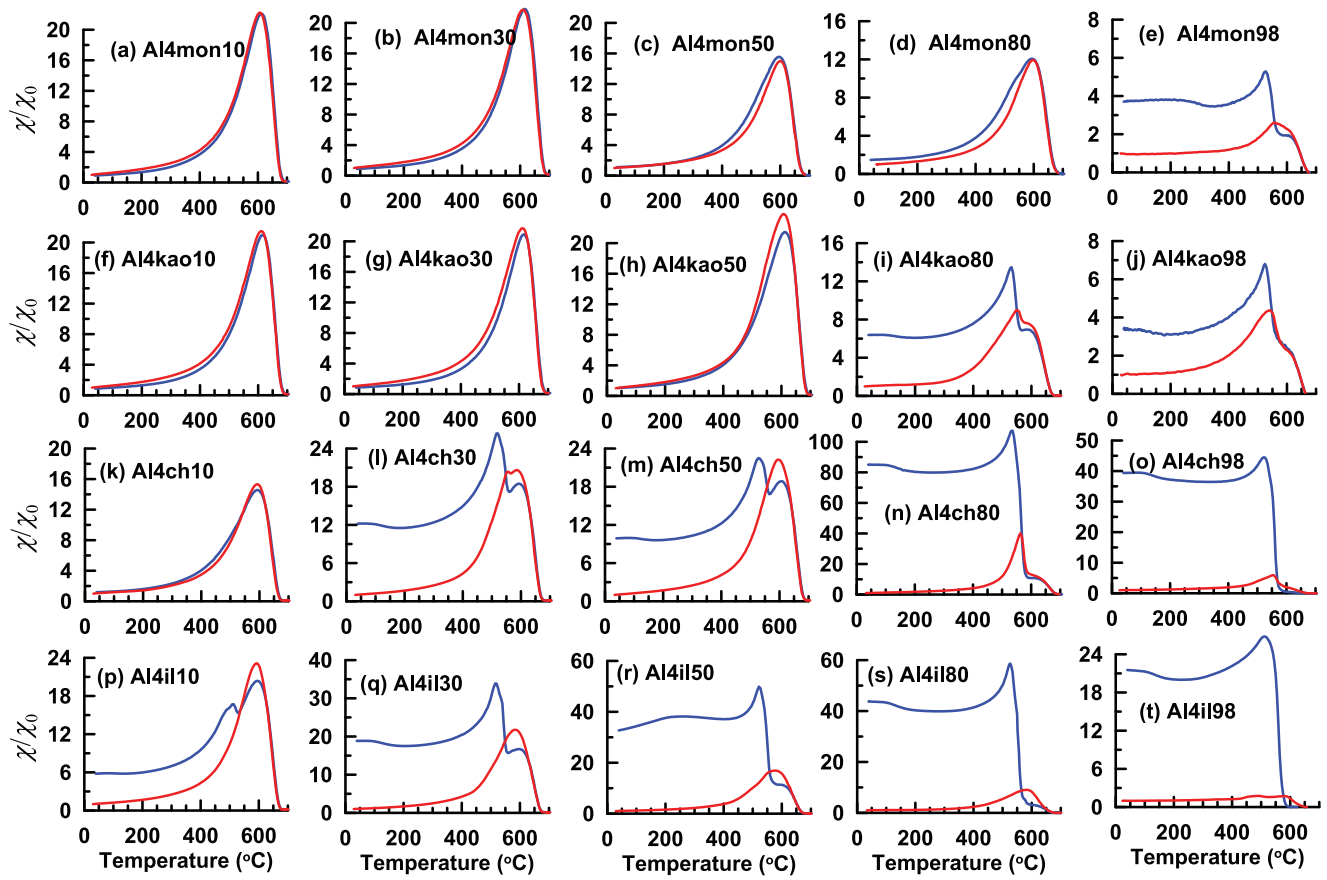

Figure 3. The χ–T curves for sample hmAl-4 mixed with different clay minerals to compare the reductive effect of these clay minerals. (a)–(e) The χ–T curves for mixtures of hmAl-4 and Ca-montmorillonite with different content, where the numbers after clay mineral represent the percentage content of clay mineral in the mixtures; (f)–(j) the χ–T curves for mixtures of hmAl-4 and kaolinite; (k)–(o) the χ–T curves for mixtures of hmAl-4 and chlorite; (p)–(t) the χ–T curves for the mixtures of hmAl-4 and illite. The red and blue lines represent the heating and cooling curves, respectively.

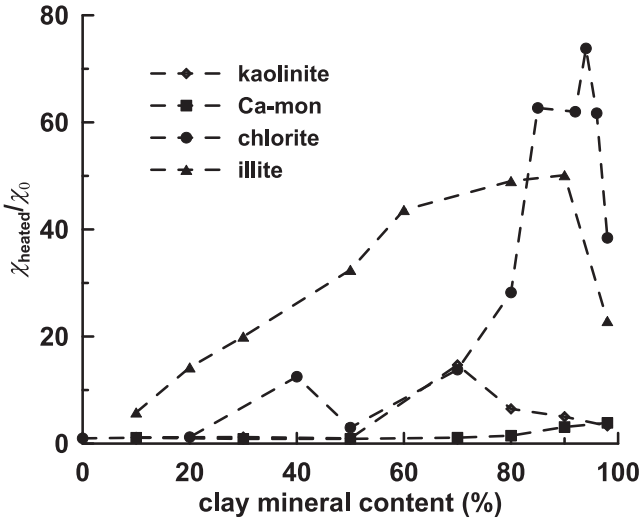

Figure 4. The diagram of the magnetic susceptibility enhancement (χ_{heated}/χ_0) versus clay mineral content, where the symbols solid diamond, square, circle, and triangle represent the mixtures of hmAl-4 with kaolinite, Ca-montmorillonite, chlorite and illite, respectively.

mol% [the ratio of Al/(Al+Fe)] and the corresponding series of samples is named HmAl-0, HmAl-4, HmAl-8 and HmAl-12. The synthetic products were washed free of salts by centrifuging the suspension, discarding the supernatant, resuspending and dialyzing the precipitation in deionized water until the electrical conductivity of the equilibrium solution <0.01 dS m^{-1}. Finally, the suspension was dried at 60 °C before it was heated at 700 °C to remove potential contaminants of goethite or akaganéite.

The concentrations of Al in the resulting samples were determined by atomic absorption spectrometry (AAS) after dissolving the samples in concentrated HCl. The purity of our samples was determined by powder X-ray diffraction (XRD) patterns that were measured on a D/MAX-2400 XRD instrument with monochromatized CuKα radiation operating at 40 kV and 40 mA. XRD diffraction patterns were measured in the range of 2–35° 2θ for clay minerals and 20–90° 2θ for haematite samples at a scan speed of 0.0167° 2θ s^{-1} with 0.1 mm divergence slit size.

A series of mixtures of Al-hm and clay minerals were prepared for magnetic measurements. The total mass of each mixed sample was kept identical (200 mg), and the mass ratio of Al-hm/mixed sample varied from 0 to 80 per cent at an interval of 10 per cent and from 80 to 98 per cent at an interval of 2 per cent. Samples HmAl-4 were mixed with four types of clay minerals, respectively, resulting in samples of Al4kao*, Al4mon*, Al4il* and Al4ch* (kao, mon, il and ch represent kaolinite, montmorillonite, illite and chlorite, respectively). In addition, the other three Al-hm series were also mixed with chlorite in the same way as HmAl-4 (Al0ch*, Al8ch* and All2ch*) to investigate the effect of Al-substitution on the reduction reactions.

The χ–T curves ranging from room temperature to 700 °C were measured using the Kappabridge MFK1-FA system (sensitivity of

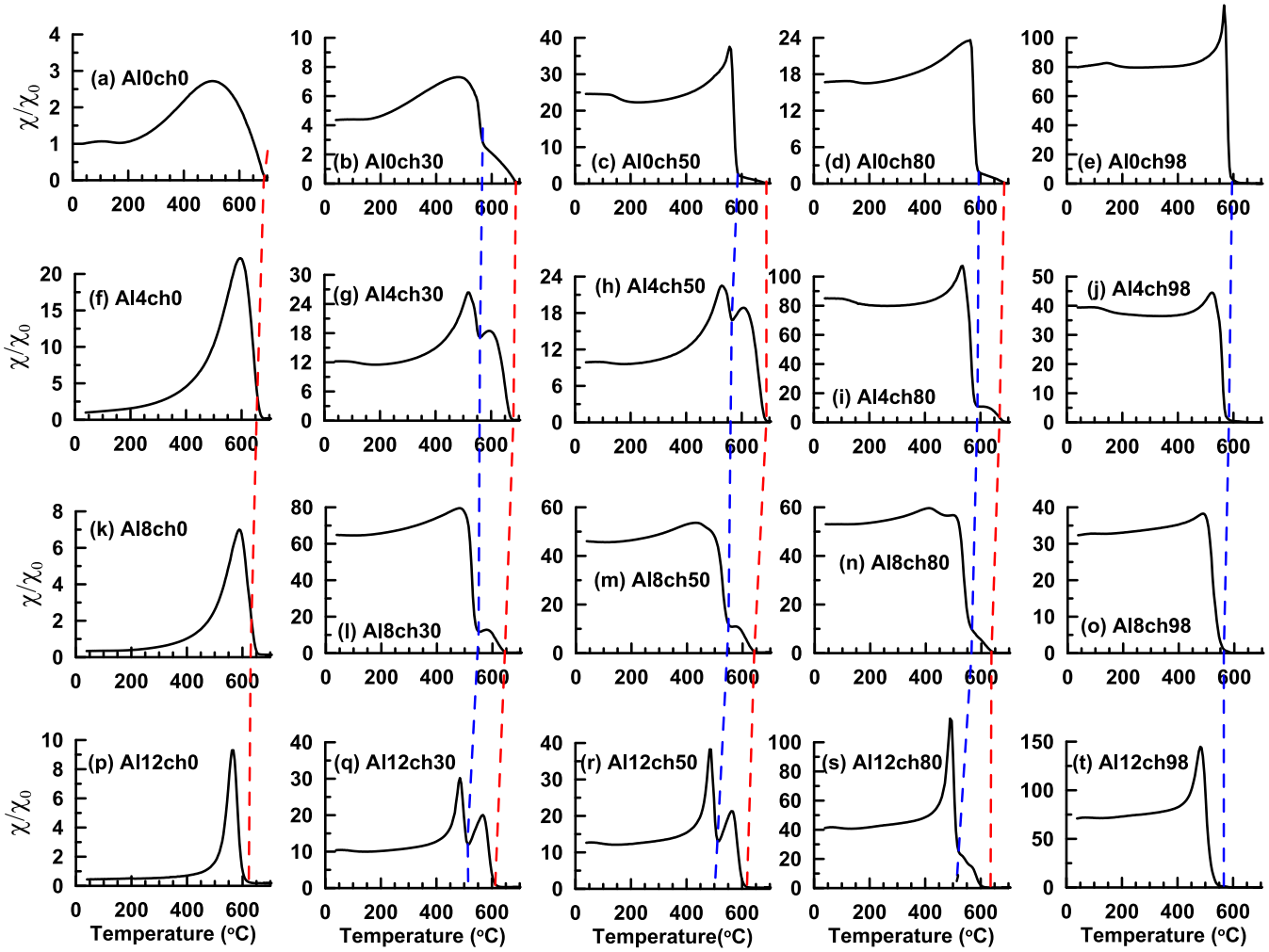

Figure 5. The cooling curves for Al-hm samples mixed with chlorite in different contents. (a)–(e) The cooling curves for mixtures of hmAl-0 and chlorite, where the numbers after 'ch' stand for the mixed chlorite content in percentage; (f)–(j) the cooling curves for mixtures of hmAl-4 and chlorite; (k)–(o) the cooling curves for mixtures of hmAl-8 and chlorite; (p)–(t) the cooling curves for mixtures of hmAl-12 and chlorite. In addition, the dash lines in red and blue represent the variation trends for Curie temperature of haematite and neo-formed magnetite, respectively.

1×10^{-8} SI, AGICO Ltd., Brno, Czech Republic) in argon environment at the frequency of 967 Hz. Minor contributions from the sample holder and thermocouple to the magnetic susceptibility were subtracted. Then T_c and/or T_N were calculated using the inverse susceptibility method ($1/\chi$; Petrovský & Kapička 2006). Magnetic hysteresis loops of these heated samples were subsequently measured in a field range of ±1.5 T using a vibrating sample magnetometer (MicroMag VSM 3900) to investigate their magnetic properties. The saturation magnetization (M_s), saturation remanence (M_{rs}) and coercivity (B_c) were determined after paramagnetic calibration. Also, the stepwise acquisition of an isothermal remanent magnetization (IRM) and backfield for the heated samples were measured with a maximum field of 1.5 T to obtain the remanent coercivity (B_{cr}). All the parameters are summarized in Table 1.

Furthermore, in order to better characterize the final magnetic minerals of the heated samples, the low temperature properties were measured on a Quantum Design Magnetic Properties Measurement System (MPMS XP-5, sensitivity 5.0×10^{-10} Am^2). Samples were first cooled from room temperature to 20 K and a field of 2.5 T was imparted at 20 K (the acquired remanence is denoted as IRM_{20K}). Then the temperature started to increase after the magnetic field was switched off, IRM_{20K} was measured from 20 to 300 K with an interval of 5 K. Additionally, some typical heated samples were also selected for XRD measurement to confirm the chemical composition.

3 RESULTS

3.1 The properties of clay minerals and Al-hm samples

The chemical analysis of the studied clay minerals is summarized in Table 2. The dominant component is SiO_2 (~50 per cent). The content of Fe decreases in the order of illite > chlorite > kaolinite > Ca-montmorillonite. The Al content in the resulting four Al-hm samples is 0, 1.8, 6.5 and 8.0 mol%, respectively. The XRD results (Fig. 1) confirm the purity of these samples. The XRD pattern shows systematic peak shift [e.g. (104) and (116) of Figs 1a–d] for Al-hm samples as the Al content increases, which is consistent with previous results (Schwertmann *et al.* 1977).

The χ–T curves of the unmixed single mineral are summarized in Fig. 2. The T_c around 585 °C indicates the existence of magnetite in the unmixed clay minerals (Figs 2a–d), which is in accord with the chemical analysis (Table 2). Moreover, the cooling curves for chlorite and illite are enhanced significantly with a four times larger

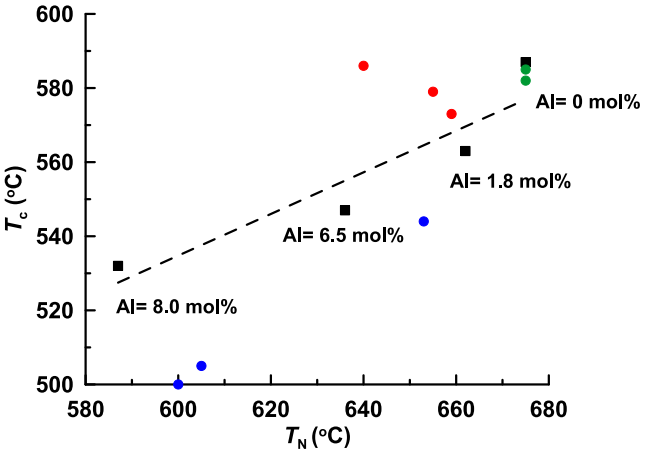

Figure 6. The diagram for Néel temperature (T_N) of haematite versus Curie temperature (T_c) of magnetite. The dashed line is the fitting curve of T_N versus T_c. The green, red and blue solid circles represent data of loess/palaeosol samples, red beds samples from Tibetan plateau, and red soil samples from the southern China, respectively.

room temperature χ (Figs 2c and d), which illustrates the neoformation of magnetite during heating. For Ca-montmorillonite, the heating and cooling curves are nearly reversible, while the cooling curve of kaolinite is even lower than the heating curve which indicates the destruction of magnetite during heating. Therefore, the χ–T results indicate that kaolinite and Ca-montmorillonite are more stable than chlorite and illite in thermal treatment in terms of formation of secondary magnetic minerals. The magnetic hysteresis loops of samples pre- and postheating further confirm that the magnetizations of chlorite and illite are enhanced remarkably after heating (Figs 2k and l), while that of Ca-montmorillonite is suppressed remarkably (Fig. 2i).

The heating and cooling curves of χ–T curves of the Al-hm samples are almost reversible (Figs 2e–h) indicating negligible mineral transformation occurs. The Néel temperature (T_N) of the Al-hm samples decreases as the Al content increases, showing an apparent dependence on the Al content. All samples except HmAl-0 have a relatively sharp distribution of blocking temperatures. Hysteresis loops of these Al-hm samples (Figs 2m–p) are not saturated even at the maximum field of 2 T, and the linear increase at high field is representative for the antiferromagnets (Jiang *et al.* 2012).

3.2 The reducing capability of different clay minerals

The χ–T curves of the mixtures of HmAl-4 with these four clay minerals are shown in Fig. 3. In general, the irreversibility of heating and cooling curves becomes enhanced as the clay mineral content increases. For kaolinite and Ca-montmorillonite, the irreversibility of heating and cooling curves are negligible until clay mineral content increases to 80 per cent (Figs 3d, e, i and j). For chlorite and illite, the alteration becomes significant even with 30%wt of clay (Figs 3i–t). As the cooling curves get enhanced, a component with T_c around 585 °C also becomes pronounced indicating the growth of magnetite. Clearly, Hopkinson peaks of magnetite can be observed in the cooling curves which demonstrates that magnetite should be in single domain state.

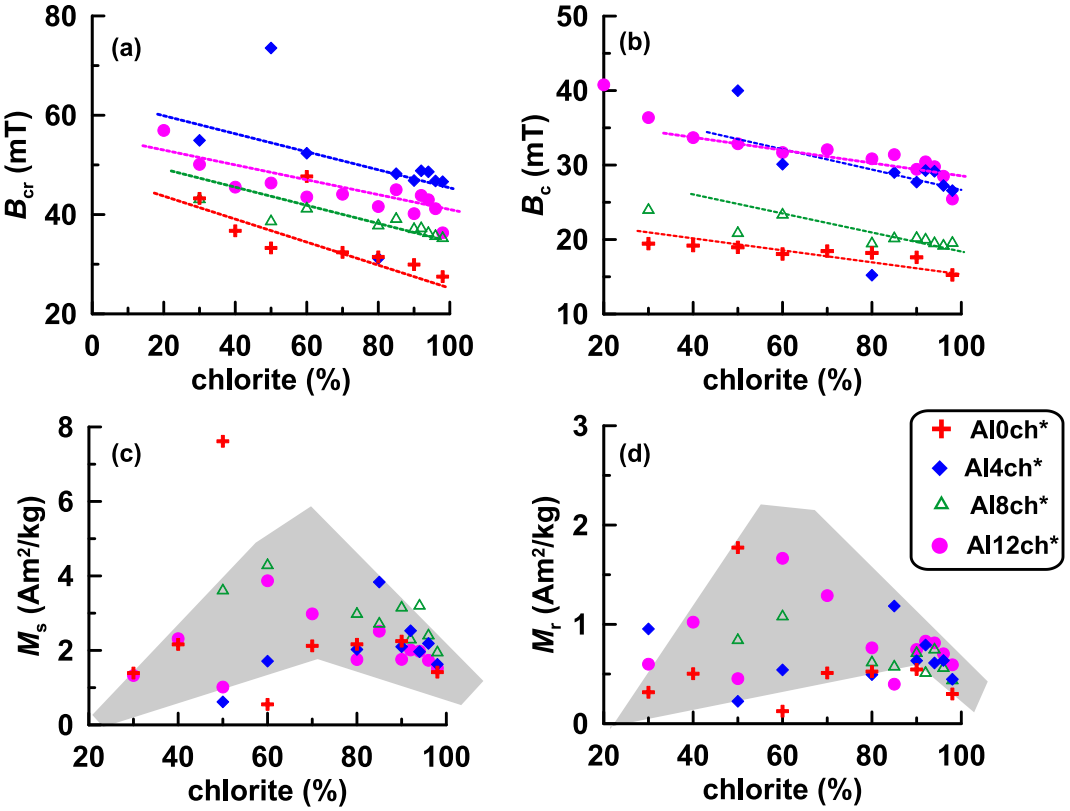

Figure 7. Correlation diagrams for magnetic parameters versus chlorite content, where the red plus, blue diamond, empty triangle, and solid circle represent mixed samples of series Al0ch*, Al4ch*, Al8ch* and Al12ch*, respectively, and the dash lines are fitting curves for these diagrams. (a) Remament coercivity (B_{cr}) versus chlorite content; (b) coercivity (B_c) versus chlorite content; (c) saturation magnetization (M_s) versus chlorite content; (d) remanent magnetization (M_r) versus chlorite content.

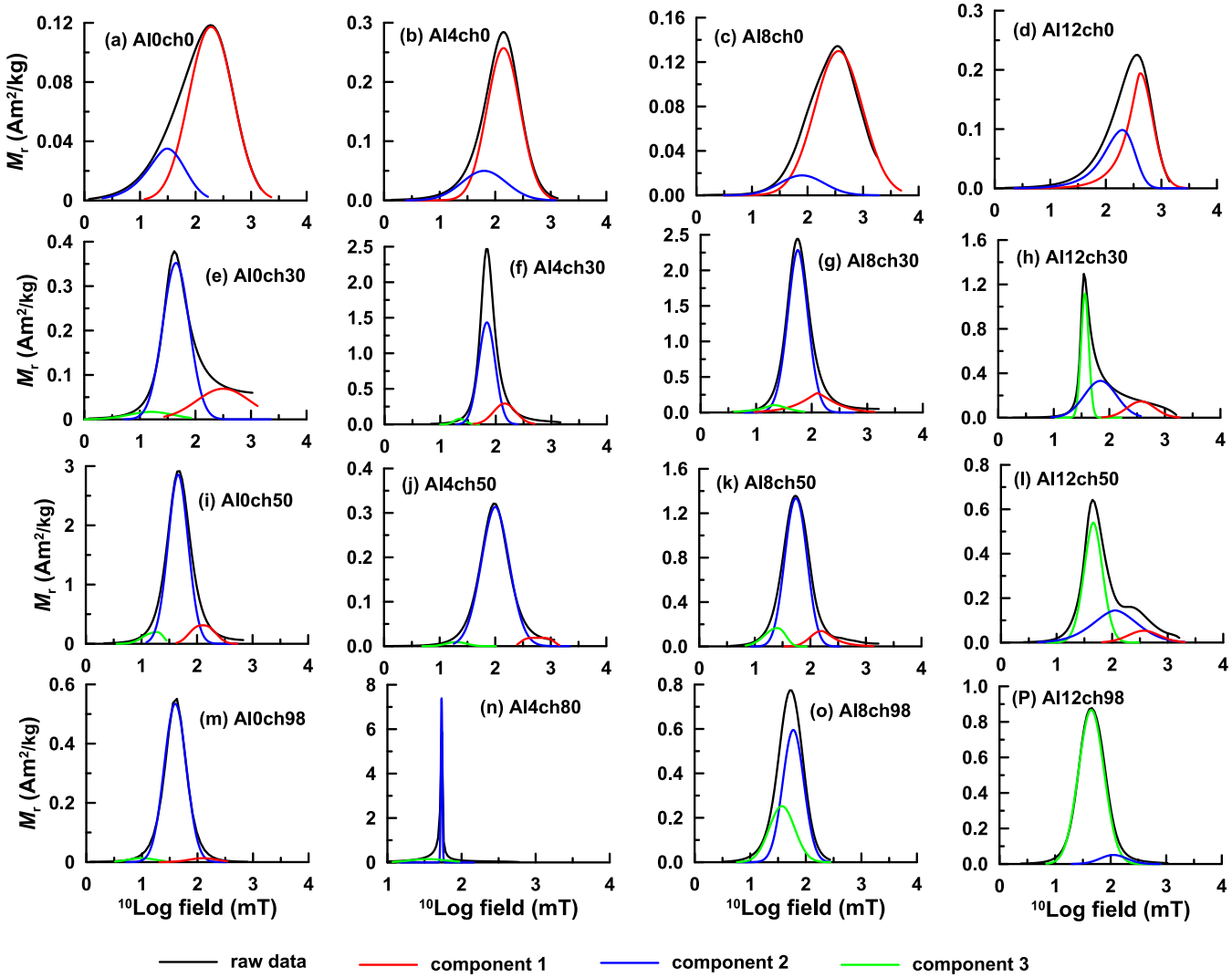

Figure 8. The isothermal remanent magnetization (IRM) component analysis for Al-hm samples mixed with different chlorite contents, where the numbers after 'Al' and after 'ch' represent Al content in mol% and chlorite content in percentage, respectively. In addition, the black, red, blue and green lines stand for raw data, component 1, component 2 and component 3 curves, respectively.

Fig. 4 illustrates the magnetic enhancement after heating (χ_{heated}/χ_0, χ_0 and χ_{heated} are magnetic susceptibilities at room temperature before and after heating, respectively) versus the content of clay minerals for the mixtures of haematite and four types of clay minerals. It demonstrates that the magnetic enhancements of haematite–chlorite and haematite–illite are remarkable compared to that of haematite–kaolinite and haematite–Ca-montmorillonite. For the mixtures of kaolinite with haematite and Ca-montmorillonite with haematite, χ_{heated}/χ_0 is around 1 until clay mineral content reaches 80 per cent, while that of haematite–chlorite and haematite–illite is close to 80. These results indicate that the reducing ability of chlorite and illite is stronger than that of kaolinite and Ca-montmorillonite. The degree of magnetic enhancement of the mixtures is a function of both the type and content of clay minerals. However, no clay mineral can reduce the haematite totally.

3.3 The effect of Al on the reduction reaction

The cooling χ–T curves for different Al-hm mixed with chlorite (Fig. 5) show that the magnetite signal becomes pronounced as chlorite content increases. Furthermore, T_c of the neo-formed magnetite becomes lower as Al content of the original Al-hm increases, which demonstrates that Al is incorporated into the structure of magnetite during the reduction of Al-hm. Therefore, the reduction product of Al-hm should be Al-substituted magnetite (Al-Mt). Fig. 6 displays the positive linear correlation of T_c of Al-Mt and T_N of Al-hm, which suggests that Al is incorporated into the structure of magnetite in proportion to that of Al-hm.

The related diagrams of hysteresis parameters (B_c, B_{cr}, M_s and M_{rs}) and chlorite content for different Al-hm samples were plotted in Fig. 7. B_c and B_{cr} are negatively correlated with chlorite content (Figs 7a and b). The mixed samples become magnetically harder as Al content increases, which can be attributed to the development of defect or internal stress arising from the incorporation of Al (Wells *et al.* 1999; Liu *et al.* 2007). Nevertheless, for all of these mixed samples, M_s or M_{rs} increase firstly and then decrease gradually as chlorite content increases, but no clear variation trend can be observed for each series of mixed samples (Figs 7c and d).

The IRM acquisition curves of the selected samples were analysed using the MAG-MIX package of (Egli 2003) to determine the magnetic coercivity distributions. Results show that the initial Al-hm samples are composed of two coercivity components:

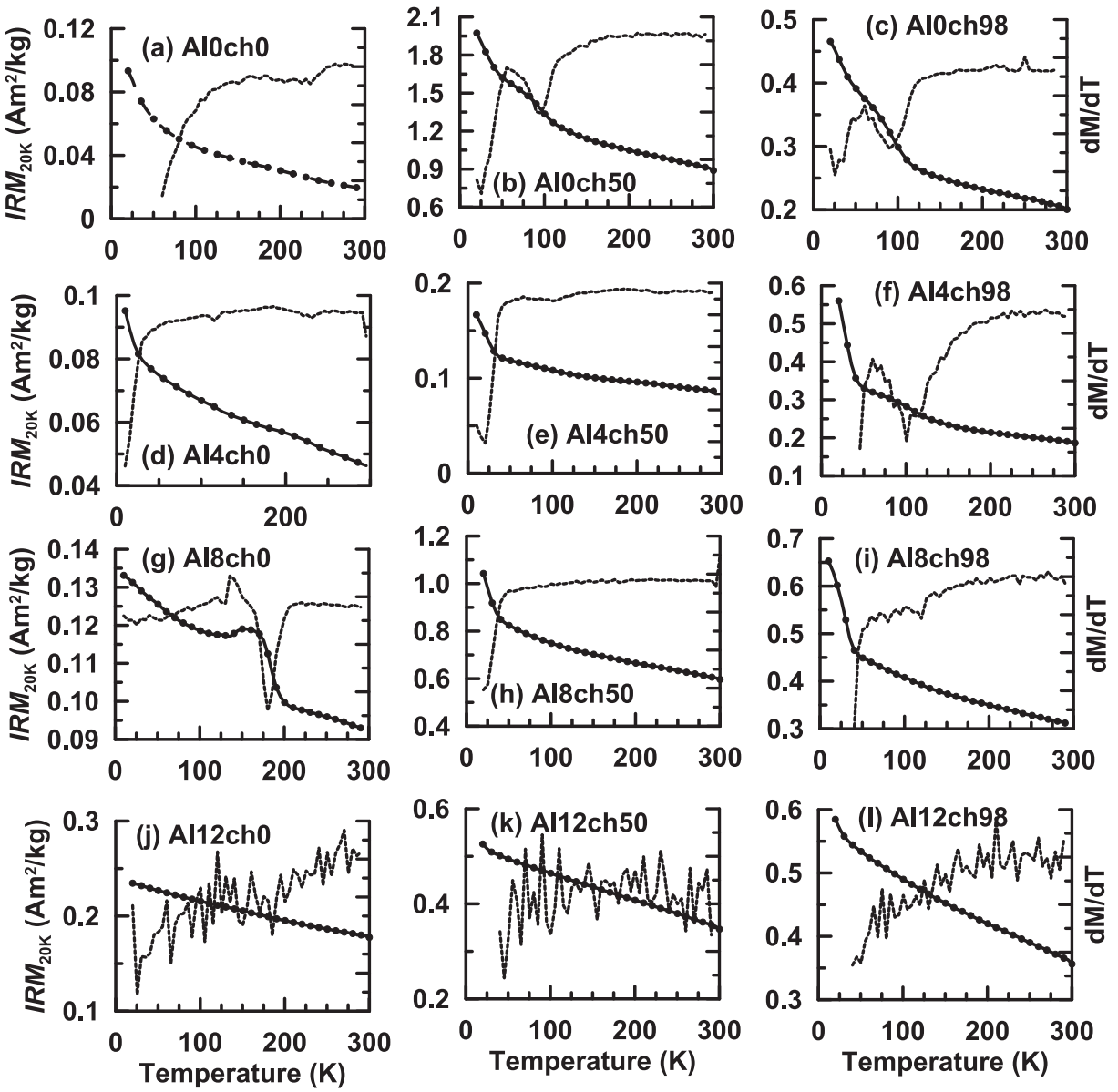

Figure 9. Temperature dependence of $SIRM_{20K}$ produced by a 5 T field applied at 20 K after zero field cooling from 300 to 20 K, where the dash lines represent the first derivative curves of $SIRM_{20K}$–*T*.

a pronounced high coercivity component around 1 T (component 1) and a less significant medium coercivity component near tens of mT (component 2; Figs 8a–d). However, as chlorite was added, the pronounced component becomes weaker and the medium component predominates, and a much softer component (component 3) is generated (Figs 8e–l). When the content of added chlorite reaches 98 per cent, the pronounced component disappears, so only two components are observed (Figs 8m–p). As a result, the bulk coercivity becomes lower as chlorite content increases, which is consistent with the hysteresis loop results. In addition, as Al content increases, Al-hm is more sensitive to chlorite, and more component 3 is produced.

Obvious Verwey transition can be observed in the heating curves of IRM_{20K} from 20 to 300 K for Al0ch* samples, which further confirms that the new formed mineral is magnetite (Figs 9a–e). However, for those mixed samples with Al-hm, no Verwey transition can be detected, which may be inhibited by Al substitution (Muxworthy & McClelland 2000). In order to trace the final minerals after heating, the XRD were measured on the heated products of Al4ch* series samples (Fig. 10). Only haematite was detected on sample Al4ch10 which contained 10 per cent chlorite initially. However, as more chlorite was added to the initial mixtures, magnetite and Na-montmorillonite were detected in the XRD spectrum of the reduced products (Fig. 10), indicating that magnetite and Na-montmorillonite are the chemical reaction products of haematite and chlorite. Finally, when chlorite content reached 98 per cent, only magnetite and Na-montmorillonite were observed. These results confirm the magnetic measurements.

4 DISCUSSION

4.1 The reduction mechanism of Al-hm samples during heating

Our results show that more magnetite was produced for mixtures of haematite and chlorite or illite, which were richer in Fe than

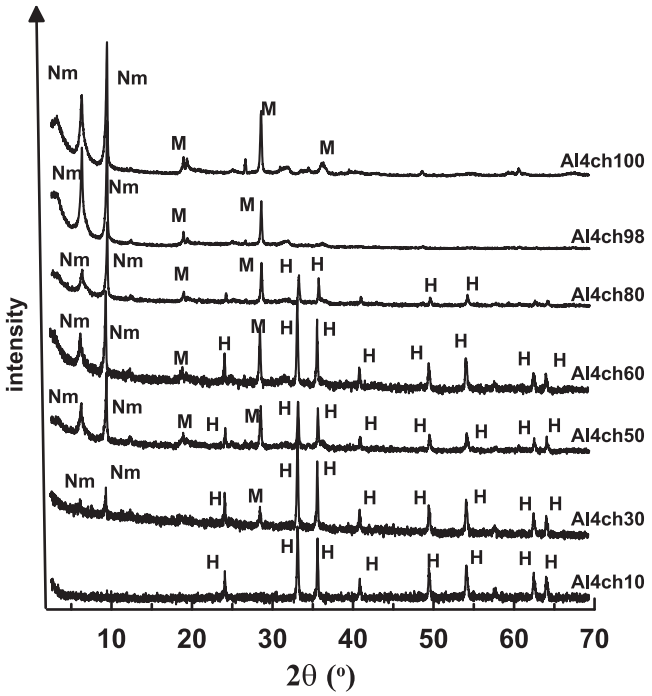

Figure 10. X-ray diffraction (XRD) spectra for thermal products of series mixed samples Al4ch* which have been heated in argon from room temperature to 700 °C and then cooling to room temperature. The XRD were measured between 2 and 70° (2θ). In addition, the labels H, M, Nm near the peaks represent haematite, magnetite and Na-montmorillonite, respectively.

that of kaolinite and Ca-montmorillonite (Table 2), which illustrates that Fe plays an important role during thermal transition (Zhang *et al.* 2010, 2012). Hirt *et al.* (1993) investigated the magnetic variation of montmorillonite during heating, and they proposed that Fe was not isolated from the structure while the stronger magnetic magnetite was transformed from the Fe salt absorbed on the surface of montmorillonite. In our experiment, chlorite ([(Mg, Fe)$_4^{2+}$ (Fe, Al)$_2^{3+}$Si$_2$O$_{10}$(OH)$_8$]) was transformed into montmorillonite ([(Na$_{0.33}$(Al$_{1.67}$Mg$_{0.33}$)Si$_4$O$_{10}$(OH)$_2$, nH$_2$O)]) during heating (Fig. 10), indicating that Fe was transferred from the structure of chlorite. The released Fe was probably adsorbed on the surface of new-formed montmorillonite and joined into the following reduction reaction.

χ–T curves showed that the new-formed magnetic mineral is magnetite. Although chlorite can release Fe out, χ of chlorite was just enhanced four times, while that of the mixture of haematite and chlorite can be enhanced by tens of times, which demonstrates that haematite was reduced into magnetite by the released Fe. Fig. 3 showed that χ in the heating curve was enhanced gradually above 500 °C, and the Hopkinson peak can be observed, while the cooling curve increases sharply and is far above the heating curve when temperature decreases to 580 °C, which indicates that the reduction reaction starts from 500 °C, and becomes more strongly above 580 °C. A series of variations occur to clay minerals during the thermal treatment, which are related with the heating rate and the stable time at the highest temperature (e.g. Hirt *et al.* 1993).

In order to better illustrate the reducing ability of different clay minerals, a proxy for the reduced haematite content, Re, was proposed. We set the initial susceptibility of the minerals mixture is $X_0 = \kappa_0 \times 10$ cm^3, where κ_0 is the volume magnetic susceptibility before heating, and the default volume of the instrument is 10 cm^3. Because the mass magnetic susceptibility of haematite (χ_{Hm}) is around $\sim 10^{-5}$ cm^3 kg^{-1} while that of clay mineral is around $\sim 10^{-8}$ cm^3 kg^{-1} (Fig. 2), then we just neglected the contribution of clay minerals to the initial magnetic susceptibility, so $X_0 = X_{Hm} = \chi_{Hm} \times m_{Hm}$, where m_{Hm} is the mass of haematite. The magnetic susceptibility of mineral mixtures after heating is $X_{heated} = \kappa_{heated} \times 10$ cm^3, where κ_{heated} is the volume magnetic susceptibility after heated. If haematite was reduced totally, then $X_{heated} = X_{mt} = \chi_{mt} \times m_{mt}$, where χ_{mt} and m_{mt} are the mass normalized magnetic susceptibility and mass of magnetite reduced from haematite. If just Re% of haematite was reduced, then $X_{heated} = \text{Re\%} \times X_{mt} + (1 - \text{Re\%}) \times X_{Hm}$. Based on this equation, we can obtain Re:

$$\text{Re} = (X_{heated} - X_0)/X_{Hm}/[X_{mt}/X_{Hm} - 1] \times 100 \text{ per cent.}$$

Fig. 11 shows that more haematite in percentage can be reduced with the increasing of clay minerals. For each series of samples, Re is near to zero until clay minerals content reaches 80 per cent, where a sharp raise occurs. For kaolinite and Ca-montmorillonite, Re is below 2 per cent in maximum, while that of chlorite and illite can reach 14 per cent, which demonstrates that chlorite and illite have more reductive capacity than either kaolinite or Ca-montmorillonite. In addition, Re is also positively related with Al substitution (Fig. 11b) indicating that Al substitution promotes the reduction of haematite. Moreover, Re is limited to 80 per cent, that is, haematite cannot be totally reduced although no haematite signal can be observed in the cooling curves of samples mixed with 98 per cent chlorite.

Based on above analysis, we conclude that the reduction of haematite is controlled by three parameters, clay mineral type, clay mineral content, and the Al substitution of haematite. The isoline map of Re (Fig. 12) shows that the higher the Fe content of clay

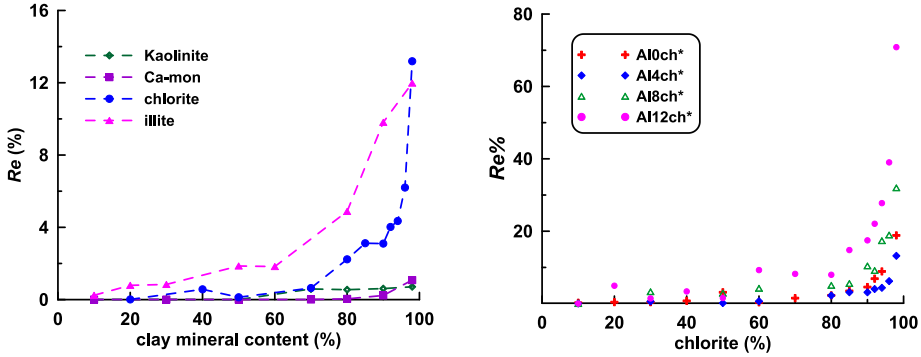

Figure 11. The diagram of haematite reduced content (Re) versus clay mineral content for mixtures of hmAl-4 with different clay minerals (a), and Re of haematite with different Al content versus chlorite content (b).

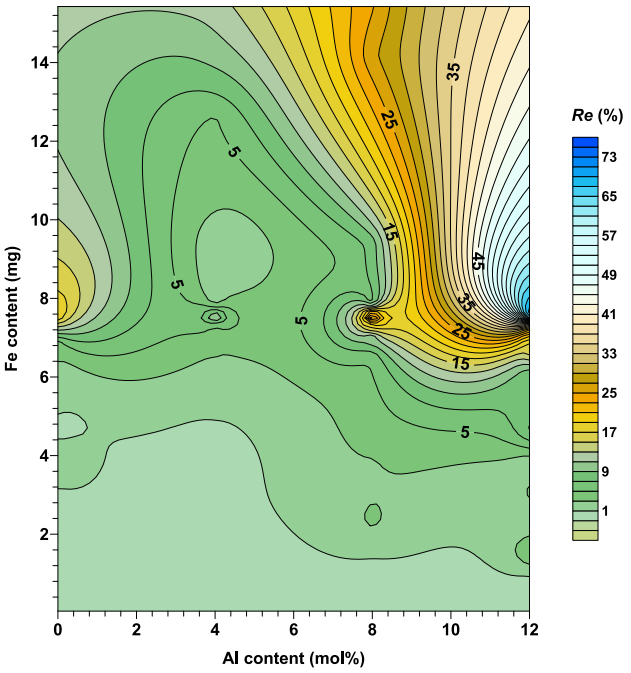

Figure 12. The contour map of Re on the plot of total iron content in clay minerals and Al substitution of haematite.

minerals and Al substitution of haematite, the higher the Re. When clay mineral content increases, the Fe content in the mixture will increase, and more Fe can be released during heating. As a result more haematite can be reduced. In addition, XRD data for haematite with different Al content indicates that the crystallinity of haematite decreases when Al content increases (Fig. 1). Lattice with lower crystallinity should be much easier to be changed during reductive reactions, which is the reason why Al substitution can promote the reducing of haematite. However, for all of mixed samples, haematite is not totally reduced, which demonstrates that clay minerals just reduce the surface of haematite, while the inside core is still haematite. In addition, no haematite can be detected by XRD on the heated product of Al4ch98, because the haematite content is too low to be detected by XRD. Figs 3 and 6 display that the T_c of the final magnetite is related to Al content, demonstrating that Al is inherited into the structure of magnetite. The T_N of the left haematite is also related with Al content, indicating that Al is also in the inner core of haematite and is distributed uniformly in the structure of haematite.

4.2 Implications for natural samples

The above results were acquired from the synthetic haematite. However, natural samples also display similar behaviours. Clay minerals are abundant in soils and sediments, and usually coexist with iron oxides (Griffin *et al.* 1968; Chamley 1989; Zhao & Zhang 1990; Thiry 2000). It is not easier to prohibit this kind of coreactions of clay minerals and iron oxides. In order to compare the thermal behaviours of the natural and synthetic samples, twelve natural samples with abundant haematite were selected from three sites distributed in different climate zone in China: Qiliting red soil sequence from the subtropical southern China (Liu *et al.* 2010), red bed samples from the Fenghuoshan area of the Tibetan Plateau, and loess/palaeosol samples from the Luochuan profile of Chinese Loess Plateau (Jin & Liu 2011). Previous study showed that the main clay minerals are kaolinite and minor illite for Qiliting red soil (Liu *et al.* 2010), illite and chlorite for red beds samples of Tibetan Plateau (Hu *et al.* 2005, 2006) and illite for loess/palaeosol samples (Ji *et al.* 1999). The different type of dominant clay minerals may be attributed to the different climate conditions of these areas. Cold and dry climate is more favourable to the preservation of illite and chlorite (Chamley 1989).

Haematite information can be detected obviously in the heating curves of red soil and red bed samples (Fig. 13), however, a majority of the haematite signal is substituted by stronger magnetite information in the cooling curves demonstrating that amount of haematite should be reduced during heating process. For loess/palaeosol samples, haematite cannot be clearly detected because of the suppression of stronger magnetic minerals (magnetite and/or maghemite). However, a substantial mass of haematite should exist which causes the colour variation of loess and palaeosols (Ji *et al.* 2002, 2004; Liu *et al.* 2007). Therefore, the magnetic enhancement of loess/palaeosol samples after heating may be attributed to the reduction of haematite by clay minerals. For all of these samples, no magnetic enhancement can be observed in the heating curves. We may deduce that this reduction should occur above 600 °C, which is consistent with the behaviour of our pure clay minerals. Thus, we consider that this magnetic enhancement may be resulted from the reduction effect of clay minerals on haematite. However, much higher magnetic enhancement occurs for red bed and loess/palaeosol samples (illite) than red soil samples (kaolinite; Fig. 13), which may be due to the higher reductive capacity of illite than that of kaolinite.

Additionally, the T_c of new-formed magnetite of these natural samples is plotted into Fig. 6. Obviously, samples from loess/plaeosols and Tibetan Plateau are close to samples without Al substitution, while samples from red soils are with Al content between 6.5 and 8 mol%, which is correlated with the climatic conditions in situ. The enrichment degree of Al, pH and temperature of the soil solutions are the prominent factors controlling Al substitution into haematite, that is, the weakly acidic or alkaline warm environment is favourable for the Al incorporation (Jiang & Liu 2012b). The red soils in the subtropical and tropical area have undergone strong chemical weathering leading to the enrichment of iron and Al (Yu & chen 1990; Gong *et al.* 2007), which results in the high Al substitution of haematite in red soils samples. Therefore, Al substitution can be used as a climatic proxy to identify different climate conditions (Cornell & Schwertmann 2003).

Finally, the ancient pottery and kilns that have recorded the palaeointensity information with high fidelity have been used as high quality materials for palaeomagnetic archeointensity studies (Dunlop & Zinn 1980; Hong *et al.* 2013). However, as these pottery and bricks were made by high temperature heated clays under ancient geomagnetic field, then a part of haematite can be neo-generated during heating process (Rodriguez & Alvarez 1999). Thus, when these materials are used for palaeomagnetic intensity studies, the haematite can be reduced by the clay minerals during the thermal demagnetization process, leading to the neoformation of magnetite, which may alter the capacity to acquire remanences and cause the pTRM tail. As a result, it is of great necessity to carry out magnetic minerals analysis by χ–T measurement before the palaeointensity experiments on ancient pottery and kilns.

5 CONCLUSIONS

In this study, the thermal magnetic investigations have been carried out on a series of synthetic Al-hm samples and Al-hm

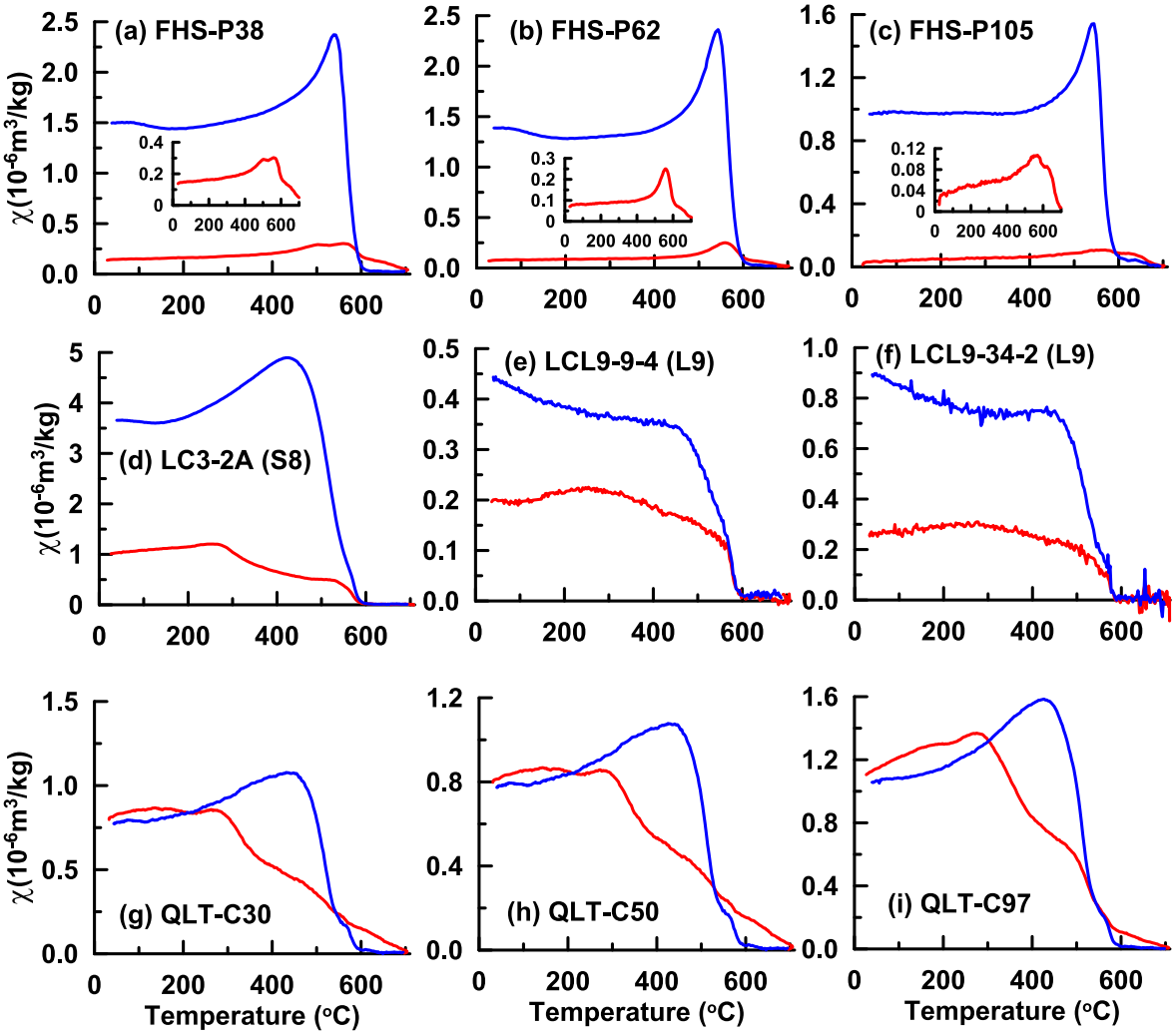

Figure 13. The χ–T curves for natural samples. The red and blue lines indicate the heating and cooling curves, respectively. (a–c) Red bed samples from Fenghuoshan (FHS) in the Tibet Plateau; the insets in (a)–(c) are the zooms of the heating curves; (d–f) loess/palaeosol samples from Luochuan profile of Chinese Loess Plateau (Jin & Liu 2011); (g–i) red soil samples from Qiliting profile of southern China (Liu *et al.* 2010).

samples mixed with different types of clay minerals. We concluded that:

(1) Al-Mt can be generated during thermal treatment, leading to significant magnetic enhancement, which is caused by the reduction effect of the clay minerals in samples. The reductive capacity differs with type of clay minerals, that is, illite > chlorite > kaolinite > Ca-montmorillonite.

(2) The iron content in the clay minerals and Al substitution of haematite are two predominant factors which control the reduced haematite content. The former one can release from the clay minerals and provide the reducing agent, while the latter one decreases the crystallinity of haematite and makes haematite easier to be reduced.

(3) The thermal magnetic measurements can be used to quantify the Al content of Al-hm in natural samples. Our study provides significant information for palaeomagnetism and environmental magnetism studies, such as thermal magnetic analysis and palaeomagnetic intensity reconstruction using ancient pottery and kilns.

ACKNOWLEDGEMENTS

Prof Claudio Colombo, Dr Hong Ao are thanked for providing the clay minerals. Dr Jianxing Liu is thanked for his meaningful discussion about this paper. This work was supported by the Natural Science Foundation of China (Grants 41374073, 41025013) and the 'Strategic Priority Research Program' of the Chinese Academy of Sciences (XDB03020102) and the National Basic Research Program of China (2013CB956403).

REFERENCES

Bailey, I., Liu, Q.S., Swann, G.E.A., Jiang, Z.X., Sun, Y., Zhao, X. & Roberts, A.P., 2011. Iron fertilisation and biogeochemical cycles in the sub-Arctic northwest Pacific during the late Pliocene intensification of northern hemisphere glaciation, *Earth planet. Sci. Lett.*, **307**, 253–265.

Bronger, A. & Heinkele, T., 1990. Mineralogical and clay mineralogical aspects of loess research, *Quat. Int.*, **7**, 37–51.

Butler, R.F., 1992. *Paleomagnetism: Magnetic Domains to Geologic Terranes*, Blackwell Scientific Publications.

Chamley, H., 1989. *Clay Sedimentology*, Springer-Verlag.

Chen, T., Xie, Q., Xu, H., Chen, J., Ji, J., Lu, H. & Balsam, W., 2010. Characteristics and formation mechanism of pedogenic hematite in Quaternary Chinese loess and paleosols, *Catena*, **81**, 217–225.

Collinson, D., 1974. The role of pigment and specularite in the remanent magnetism of red sandstones, *Geophys. J. R. astr. Soc.*, **38**, 253–264.

Cornell, R. & Schwertmann, U., 2003. *The Iron Oxides*, VCH Weinheim.

Deng, C., Zhu, R., Verosub, K., Singer, M. & Yuan, B., 2000. Paleoclimatic significance of the temperature-dependent susceptibility of Holocene Loess along a NW-SE transect in the Chinese Loess Plateau, *Geophys. Res. Lett.*, **27**, 3715–3718.

Deng, C., Zhu, R., Jackson, M., Verosub, K. & Singer, M., 2001. Variability of the temperature-dependent susceptibility of the Holocene eolian deposits in the Chinese loess plateau: a pedogenesis indicator, *Phys. Chem. Earth Part A.*, **26**, 873–878.

Dunlop, D.J. & Özdemir, Ö., 2001. *Rock Magnetism: Fundamentals and Frontiers*, Cambridge Univ. Press.

Dunlop, D.J. & Zinn, M.B., 1980. Archeomagnetism of a 19th century pottery kiln near Jordan, Ontario, *Can. J. Earth Sci.*, **17**, 1275–1285.

Egli, R., 2003. Analysis of the field dependence of remanent magnetization curves, *J. geophys. Res.*, **108**(B2), 2081, doi:10.1029/2002JB002023.

Fabian, K., Shcherbakov, V. & McEnroe, S., 2013. Measuring the Curie temperature, *Geochem. Geophys. Geosyst.*, **14**, 947–961.

Gong, Z.T., Zhang, G.L. & Chen, Z., 2007. *Pedogenesis and Soil Taxonomy*, Science Press.

Griffin, J.J., Windom, H. & Goldberg, E.D., 1968. The distribution of clay minerals in the World Ocean, *Deep Sea Res.*, **15**, 433–459.

Hanesch, M., Stanjek, H. & Petersen, N., 2006. Thermomagnetic measurements of soil iron minerals: the role of organic carbon, *Geophys. J. Int.*, **165**, 53–61.

Hirt, A., Banin, A. & Gehring, A., 1993. Thermal generation of ferromagnetic minerals from iron-enriched smectites, *Geophys. J. Int.*, **115**, 1161–1168.

Hong, H., Yu, Y., Lee, C.H., Kim, R.H., Park, J., Doh, S.-J., Kim, W. & Sung, H., 2013. Globally strong geomagnetic field intensity circa 3000 years ago, *Earth planet. Sci. Lett.*, **383**, 142–152.

Hu, X., Jansa, L., Wang, C., Sarti, M., Bak, K., Wagreich, M., Michalik, J. & Soták, J., 2005. Upper Cretaceous oceanic red beds (CORBs) in the Tethys: occurrences, lithofacies, age, and environments, *Cretaceous Res.*, **26**, 3–20.

Hu, X., Wang, C., Li, X. & Jansa, L., 2006. Upper Cretaceous oceanic red beds in southern Tibet: Lithofacies, environments and colour origin, *Sci. China Ser. D Earth Sci.*, **49**, 785–795.

Jackson, M., 1959. Frequency distribution of clay minerals in major great soil groups as related to the factors of soil formation, in *Proceeding of the 6th National Clay Conference*, Pergamon Press, New York, NY, pp. 133–143.

Ji, J., Chen, J. & Lu, H., 1999. Origin of illite in the loess from the Luochuan area, Loess Plateau, Central China, *Clay Miner.*, **34**, 525–532.

Ji, J., Balsam, W., Chen, J. & Liu, L., 2002. Rapid and quantitative measurement of hematite and goethite in the Chinese loess-paleosol sequence by diffuse reflectance spectroscopy, *Clays Clay Miner.*, **50**, 208–216.

Ji, J., Chen, J., Balsam, W., Lu, H., Sun, Y. & Xu, H., 2004. High resolution hematite/goethite records from Chinese loess sequences for the last glacial-interglacial cycle: rapid climatic response of the East Asian Monsoon to the tropical Pacific, *Geophys. Res. Lett.*, **31**, L03207, doi:10.1029/2003GL018975.

Jiang, Z.X. & Liu, Q.S., 2012a. Magnetic characterization and paleoclimatic significances of late Pliocene-early Pleistocene sediments at site 882A, northwestern Pacific Ocean, *Sci. China Ser. D Earth Sci.*, **55**, 323–331.

Jiang, Z.X. & Liu, Q.S., 2012b. Factors controlling the Al content in Al-substituted hematite and its environmental significances, *Quarter. Sci. (in Chinese)*, **32**, 608–614.

Jiang, Z.X., Liu, Q.S., Barrón, V., Torrent, J. & Yu, Y., 2012. Magnetic discrimination between Al-substituted hematites synthesized by hydrothermal and thermal dehydration methods and its geological significance, *J. geophys. Res.*, **117**, B02102, doi:10.1029/2011JB008605.

Jin, C. & Liu, Q.S., 2011. Remagnetization mechanism and a new age model for L9 in Chinese loess, *Phys. Earth planet. Int.*, **187**, 261–275.

Kiipli, E., Kallaste, T. & Kiipli, T., 2000. Hematite and goethite in Telychian marine red beds of the East Baltic, *GFF*, **122**, 281–286.

Liu, C.C., Deng, C.L., Liu, Q.S., Zheng, L., Wang, W., Xu, X., Huang, S. & Yuan, B., 2010. Mineral magnetism to probe into the nature of palaeomagnetic signals of subtropical red soil sequences in southern China, *Geophys. J. Int.*, **181**, 1395–1410.

Liu, C.Y., Ge, K., Zhang, C.X., Liu, Q.S., Deng, C.L. & Zhu, R.X., 2011. Nature of remagnetization of Lower Triassic red beds in southwestern China, *Geophys. J. Int.*, **187**, 1237–1249.

Liu, Q.S., Deng, C.L., Yu, Y., Torrent, J., Jackson, M., Banerjee, S. & Zhu, R., 2005. Temperature dependence of magnetic susceptibility in an argon environment: implications for pedogenesis of Chinese loess/palaeosols, *Geophys. J. Int.*, **161**, 102–112.

Liu, Q.S., Roberts, A.P., Torrent, J., Horng, C.S. & Larrasoaña, J.C., 2007. What do the HIRM and S-ratio really measure in environmental magnetism?, *Geochem. Geophys. Geosyst.*, **8**, Q09011, doi:10.1029/2007GC001717.

Liu, Q.S., Roberts, A.P., Larrasoaña, J.C., Banerjee, S.K., Guyodo, Y., Tauxe, L. & Oldfield, F., 2012. Environmental magnetism: principles and applications, *Rev. Geophys.*, **50**, RG4002, doi:10.1029/2012RG000393.

Minyuk, P., Subbotnikova, T. & Plyashkevich, A., 2011. Measurements of thermal magnetic susceptibility of hematite and goethite, *Izv. Phys. Solid Earth*, **47**, 762–774.

Murad, E. & Schwertmann, U., 1986. Influence of A1 substitution and crystal size on the room-temperature Mössbauer spectrum of hematite, *Clays Clay Miner.*, **34**, 1–6.

Muxworthy, A. & McClelland, E., 2000. Review of the low-temperature magnetic properties of magnetite from a rock magnetic perspective, *Geophys. J. Int.*, **140**, 101–114.

Ortega, B., Caballero, M., Lozano, S., Vilaclara, G. & Rodríguez, A., 2006. Rock magnetic and geochemical proxies for iron mineral diagenesis in a tropical lake: Lago Verde, Los Tuxtlas, East-Central Mexico, *Earth planet. Sci. Lett.*, **250**, 444–458.

Özdemir, Ö. & Dunlop, D.J., 1993. Chemical remanent magnetization during gamma-FeOOH phase transformations, *J. geophys. Res.*, **98**, 4191–4198.

Peng, S. & Guo, Z.T., 2007. Clay mineral composition of the tertiary red clay and the quaternaty Loess-Paleosols as well as its environmental implication, *Quarter. Sci. (in Chinese)*, **27**, 277–285.

Petrovský, E. & Kapička, A., 2006. On determination of the Curie point from thermomagnetic curves, *J. geophys. Res.*, **111**, B12S27, doi:10.1029/2006JB004507.

Roberts, A.P., 1995. Magnetic properties of sedimentary greigite (Fe_3S_4), *Earth planet. Sci. Lett.*, **134**, 227–236.

Rodriguez, M.C.B. & Alvarez, V.C., 1999. A preliminary archaeomagnetic study of prehistoric Amerindian pottery from Venezuela, *Interciencia*, **24**, 293–299.

Schwertmann, U., Fitzpatrick, R.W. & Le Roux, J., 1977. Al substitution and different disorder in soil hematites, *Clays Clay Miner.*, **25**, 373–374.

Su, Y. *et al.*, 2012. Mineral magnetic study of lacustrine sediments from Lake Pumoyum Co, southern Tibet, over the last 19 ka and paleoenvironmental significance, *Tectonophysics*, **588**, 209–221.

Sugimoto, T. & Sakata, K., 1992. Preparation of monodisperse pseudocubic [alpha]-Fe_2O_3 particles from condensed ferric hydroxide gel, *J. Colloid Inter. Sci.*, **152**, 587–590.

Tauxe, L., 2010. *Essentials of Paleomagnetism*, University of California Press.

Thiry, M., 2000. Palaeoclimatic interpretation of clay minerals in marine deposits: an outlook from the continental origin, *Earth Sci. Rev.*, **49**, 201–221.

Walker, T.R., 1967. Formation of red beds in modern and ancient deserts, *Geol. Soc. Am. Bull.*, **78**, 353–368.

Wells, M., Fitzpatrick, R., Gilkes, R. & Dobson, J., 1999. Magnetic properties of metal-substituted haematite, *Geophys. J. Int.*, **138**, 571–580.

Yu, T.R. & Chen, Z.C., 1990. *The Chemical Process During Soil Genesis*, Science Press.

Zhang, C.X., Liu, Q.S., Huang, B.C. & Su, Y.L., 2010. Magnetic enhancement upon heating of environmentally polluted

samples containing haematite and iron, *Geophys. J. Int.*, **181**, 1381–1394.

Zhang, C.X., Paterson, G.A. & Liu, Q.S., 2012. A new mechanism for the magnetic enhancement of hematite during heating: the role of clay minerals, *Stud. Geophys. Geod.*, **56**, doi:10.1007/s11200-011-0018-1.

Zhao, L., Ji, J., Chen, J., Liu, L., Chen, Y. & Balsam, W., 2005. Variations of illite/chlorite ratio in Chinese loess sections during the last glacial and interglacial cycle: implications for monsoon reconstruction, *Geophys. Res. Lett.*, **32**, L20718, doi:10.1029/2005GL024145.

Zhao, X. & Zhang, Y., 1990. *Clay Minerals and Clay Mineral Analysis*, Ocean Press.